ACS APPLIED MATERIALS & INTERFACES

Research Article

www.acsami.org

Improving Osteointegration and Osteogenesis of Three-Dimensional Porous Ti6Al4V Scaffolds by Polydopamine-Assisted Biomimetic Hydroxyapatite Coating

Yong Li,[†,§] Wei Yang,[†,§] Xiaokang Li,[†,§] Xing Zhang,[‡] Cairu Wang,[†] Xiangfei Meng,[†] Yifeng Pei,[†] Xiangli Fan,[†] Pingheng Lan,[†] Chunhui Wang,[†] Xiaojie Li,[†] and Zheng Guo*[,†]

[†]Department of Orthopedics, Xijing Hospital, Fourth Military Medical University, Xi'an, Shaanxi 710032, People's Republic of China

[‡]Shenyang National Laboratory for Materials Science, Institute of Metal Research, Chinese Academy of Sciences, Shenyang, Liaoning 110016, People's Republic of China

Supporting Information

ABSTRACT: Titanium alloys with various porous structures can be fabricated by advanced additive manufacturing techniques, which are attractive for use as scaffolds for bone defect repair. However, modification of the scaffold surfaces, particularly inner surfaces, is critical to improve the osteointegration of these scaffolds. In this study, a biomimetic approach was employed to construct polydopamine-assisted hydroxyapatite coating (HA/pDA) onto porous Ti6Al4V scaffolds fabricated by the electron beam melting method. The surface modification was characterized with the field emission scanning electron microscopy, energy dispersive spectroscopy, water contact angle measurement, and confocal laser scanning microscopy. Attachment and proliferation of MC3T3-E1 cells on the scaffold surface were significantly enhanced by the HA/pDA coating compared to the unmodified surfaces. Additionally, MC3T3-E1 cells grown on the HA/pDA-coated Ti6Al4V scaffolds displayed significantly higher expression of runt-related transcription factor-2, alkaline phosphatase, osteocalcin, osteopontin, and collagen type-1 compared with bare Ti6Al4V scaffolds after culture for 14 days. Moreover, microcomputed tomography analysis and Van-Gieson staining of histological sections showed that HA/pDA coating on surfaces of porous Ti6Al4V scaffolds enhanced osteointegration and significantly promoted bone regeneration after implantation in rabbit femoral condylar defects for 4 and 12 weeks. Therefore, this study provides an alternative to biofunctionalized porous Ti6Al4V scaffolds with improved osteointegration and osteogenesis functions for orthopedic applications.

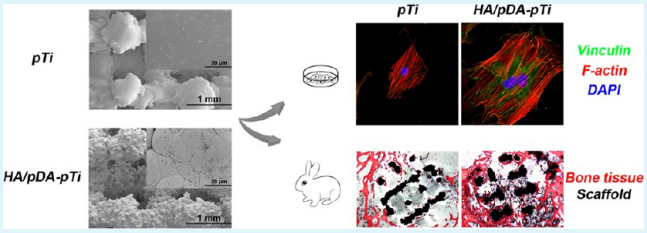

KEYWORDS: *porous titanium, surface modification, polydopamine, hydroxyapatite, osteogenesis, osteointegration*

1. INTRODUCTION

In clinical practice, autogenous and allogeneic bone have been widely used for repair of bone defects caused by trauma, tumor resection, or congenital diseases.[1] However, the application of autogenous and allogeneic bone graft is limited due to the supply shortage, donor-site morbidity, and potential of disease transmission.[1,2] Therefore, artificial bone substitutes have drawn great attention. Among them, titanium (Ti) alloys have been widely used in clinical practice because of their excellent biocompatibility, corrosion resistance property, and high mechanical strength.

Porous Ti scaffolds compared with their dense counterparts show advantages of great connectivity, high surface area, appropriate mechanical strength, and elastic modulus and are thus promising for bone defect repair. Moreover, the porous structures at the presence of interconnected pores can promote the nutrient diffusion, and therefore facilitate the newly formed bone to grow into the scaffolds.[3,4] Three-dimensional (3D) porous titanium scaffolds with fully interconnected pores, adjustable pore sizes, and appropriate mechanical properties can now be fabricated using the additive manufacturing techniques such as selective laser sintering (SLS),[5−7] selective laser melting (SLM),[8−10] and electron beam melting (EBM).[11,12]

Nevertheless, Ti implants may fail due to insufficient integration into surrounding bone. Hydroxyapatite (HA) coating is commonly employed to improve osteoconductivity and osteointegration of Ti scaffolds, which can mimic the nanoscale architecture and chemical composition of native bone mineral.[13−19] Physical deposition technique and biomimetic coating process are two commonly used approaches to fabricating HA-coating on Ti scaffolds. HA deposition rates from physical deposition techniques such as plasma spraying, pulsed laser evaporation, ion-beam-assisted deposition, and electrospray deposition are relatively high. However, it is difficult to obtain a uniform coating on the internal surfaces of porous Ti scaffolds using these techniques. In contrast, a biomimetic coating process

Received: November 6, 2014
Accepted: February 25, 2015
Published: February 25, 2015

DOI: 10.1021/acsami.5b00331
ACS Appl. Mater. Interfaces 2015, 7, 5715−5724

using a solution to resemble the inorganic nature of body fluids is beneficial to obtaining a dense, uniform coating of bone-like apatite to porous structures, but at a relatively low coating rate. Electrodeposition was also capable to produce homogeneous coating on porous structure, and the process was faster. However, the coating was easier to deposit on the outer surface due to a higher electrochemical reaction rate, the resulted coating was not homogeneous compared with biomimetic process, and the process was not mild compared with biomimetic process. Proper surface modification is generally essential to accelerate the biomimetic coating of HA. Therefore, how to modify the surfaces of porous Ti scaffolds is critical to improve HA coating formed by the biomimetic coating process.

Inspired by mussel-adhesion phenomena in nature, polydopamine (pDA) coating can be formed by dopamine self-polymerization via simple experimental procedures at mild reaction conditions, which can be used as surface modification for a variety of applications,[20] such as antibacterial treatment,[21,22] protein conjugation,[23−28] cell culture,[29−33] drug delivery,[34] and many others.[35−40] Especially, pDA coating can be applied to the internal surfaces of complex porous structures. The pDA coating at the presence of abundant catecholamine moieties was found to facilitate HA formation on various scaffolds.[41,42] In addition, HA formed on the pDA coating enhanced adhesion of preosteoblasts to porous polycaprolactone (PCL) scaffolds.[32] However, the in vivo performance of the resulting scaffold has not been investigated yet.

In this study, pDA coating was first employed to modify the surfaces of porous Ti6Al4V scaffolds fabricated by the EBM method. HA coating was then performed using a biomimetic process by immersing the pDA-coated Ti6Al4V scaffolds into the 1.5 times concentrated simulated body fluid (1.5× SBF). The interaction between preosteoblast cells (MC3T3-E1) and the porous Ti6Al4V scaffolds with or without the HA/pDA coating and osteointegration and osteogenesis properties of these scaffolds were further evaluated.

2. MATERIALS AND METHODS

2.1. Preparation of Porous Ti6Al4V Scaffolds. Porous Ti6Al4V scaffolds (pTi) were fabricated by an EBM system (Arcam A1, Arcam AB, Mölndal, Sweden) through an additive manufacturing approach as previously described (porosity, 68 ± 5.3%; pore size, 710 ± 42 μm).[11] Briefly, a 3D model was designed with CAD software. The STL data converted from CAD data was then transferred to the EBM machine. Medical-grade Ti6Al4V powder with an average diameter of ∼30 μm was preheated to 650 °C. Electron beam scanning was utilized to generate a cross section layer by fusing the powder together. Subsequently, a new layer of powder was applied, and the process was repeated until the whole construct had been built. The process was performed under vacuum (∼10^{-4} to 10^{-5} mbar). Disk-shaped samples (Ø12 mm × H2 mm) were used for in vitro assays and cylindrical samples (Ø5 mm × L10 mm) were used for in vivo experiments. All samples were ultrasonically cleaned sequentially in acetone, ethyl alcohol, and deionized water ∼15 min for each treatment.

2.2. Surface Modification of Porous Ti6Al4V Scaffolds. For polydopamine (pDA) coating, pTi were immersed into a dopamine solution (2 mg/mL in 10 mM Tris, pH 8.5) for 16 h at 25 °C. After the pDA-coating process, the scaffolds were washed with deionized water to remove the unattached dopamine and then dried with nitrogen gas. For HA coating process, the pDA-coated Ti6Al4V scaffolds (pDA-Ti) were immersed into 1.5× SBF and incubated at 36.5 °C for 2 weeks. The 1.5× SBF was prepared as previously described,[43] and the composition was as follows (× 10^{-3} mM): Na^+, 213.0; K^+, 7.5; Mg^{2+}, 2.25; Ca^{2+}, 3.75; Cl^-, 221.7; HCO_3^-, 6.3; HPO_4^{2-}, 1.5; SO_4^{2-}, 0.75. After immersion, the HA/pDA-coated porous Ti6Al4V scaffolds (HA/pDA-pTi) were rinsed with deionized water and dried by nitrogen gas.

2.3. Characterization. The morphology of sample surface and cross-section was characterized by the field emission scanning electron microscopy (FE-SEM, S-4800, HITACHI, Japan). Elements energy dispersive spectroscopic (EDS) analysis was performed to identify the chemical composition of the samples using EMAX. Before the detection, samples were sputtered with a thin layer of platinum (Pt) using a common sputtering instrument to improve the surface conductivity. Water contact angle was performed using a contact angle goniometer (Dataphysics, Germany). Briefly, 10 μL of deionized water was dropped onto the sample surfaces. The shape of the water drop was captured and measured using SCA20 software (Dataphysics, Germany). The surface roughness of the samples was detected using an Olympus confocal laser scanning microscope (OLS4000, Japan). Mechanical stability of pDA and HA coating was evaluated using ultrasonication test (40 kHz) and peeling test as previously described.[42] The HA/pDA-pTi samples (immersed into SBF for 2 days) were treated with ultrasonication test for an hour and peeling test pressing a piece of Scotch tape (3M#610) down firmly on the samples and removing it quickly, and the amounts of HA on the substrate before and after ultrasonication and peeling test were compared. To better investigate the change of wettability, roughness, and coating mechanical stability, we used solid Ti6Al4V substrates instead of porous Ti6Al4V scaffolds.

2.4. Cell Culture. Mouse preosteoblast cells (MC3T3-E1) were cultured in complete medium (α-MEM medium supplemental with 10% fetal bovine serum, 100 U/ml penicillin and 100 μg/mL streptomycin) in a humidified incubator at 37 °C with 5% CO_2. The medium was changed every 2 days.

2.5. Cell Proliferation and Morphology. The MC3T3-E1 cells were seeded on the samples (bare pTi, pDA-pTi, and HA/pDA-pTi) at a density of 5 × 10^4/well in 24-well culture plates and cultured for 1, 4, and 7 days to evaluate the cell proliferation using cell count kit-8 (CCK-8, Dojindo, Japan). Briefly, at each time point, the samples were transferred to new 24-well culture plates. CCK-8 solution with a 10% volume of the medium was then added into the wells, and the samples were incubated at 37 °C for 2 h. Then, 100 μL of the reaction solution was transferred into a new 96-well plate, and the optical density was measured at 450 nm by a microplate reader.

The MC3T3-E1 cells were seeded on the samples (bare pTi and HA/pDA-pTi) at a density of 5 × 10^4/well in 24-well culture plates. After incubation for 48 h, samples were fixed using 4% paraformaldehyde (PFA) in PBS for 15 min, and permeabilized with 0.1% Triton-X 100 in PBS for 5 min. After being blocked with 1% bovine serum albumin (BSA) in PBS for 30 min, samples were incubated with primary antibody against vinculin (1:200, Abcam) at 4 °C overnight. Subsequently, samples were washed with PBS three times and then incubated with fluorescein isothiocyanate (FITC)-conjugated goat antirabbit secondary antibody (1:100) at room temperature (RT) for 1 h. After the vinculin staining process, samples were stained with rhodamine-phalloidin (Cytoskeleton, Inc.) for 30 min at RT for visualization of filamentous actin (F-actin), and nuclei were counterstained with 4′,6 diamidino-2-phenylindole (DAPI). Images were captured using an Olympus confocal laser scanning microscope. The cell overall area to the nucleus area (CN ratio) and vinculin expression were measured using the ImageJ software.

The MC3T3-E1 cells were seeded on the samples (bare pTi and HA/pDA-pTi) at a density of 5 × 10^4/well in 24-well culture plates. After incubation for 4 days, the samples were washed with PBS and fixed in 2.5% v/v glutaraldehyde at 4 °C overnight. Then, the samples were dehydrated through an ethanol series, critical-point dried, and sputtered with Pt. The samples were observed using the FE-SEM (S-4800, HITACHI, Japan).

2.6. Quantitative Real-Time PCR (RT-PCR). The MC3T3-E1 cells were seeded on the samples (bare pTi and HA/pDA-pTi) at a density of 5 × 10^4/well in 24-well culture plates. After cell adherence, the cells were cultured using osteogenic medium (complete medium supplemented with 50 mg/L ascorbic acid and 10 mM β-glycerol phosphate). The medium was changed every 2 days. After osteogenic medium treatment for 7 and 14 days, the expression of runt-related transcription factor-2 (Runx2), alkaline phosphatase (ALP), osteocalcin (OCN), osteopontin

DOI: 10.1021/acsami.5b00331
ACS Appl. Mater. Interfaces 2015, 7, 5715−5724

Table 1. Primers Used in Real-Time PCR

gene	forward primer sequence (5′- 3′)	reverse primer sequence (5′- 3′)
GAPDH	TGCTGGTGCTGAGTATGTGGT	AGTCTTCTGGGTGGCAGTGAT
Runx2	GAACCAAGAAGGCACAGACAGA	GGCGGGACACCTACTCTCATAC
ALP	TTGGGCAGGCAAGACACA	GAAGGGAAGGGATGGAGGAG
OCN	ACCATCTTTCTGCTCACTCTGCT	CCTTATTGCCCTCCTGCTTG
OPN	TACGACCATGAGATTGGCAGTGA	TATAGGATCTGGGTGCAGGCTGTAA
Col-1	GACATGTTCAGCTTTGTGGACCTC	GGGACCCTTAGGCCATTGTGTA

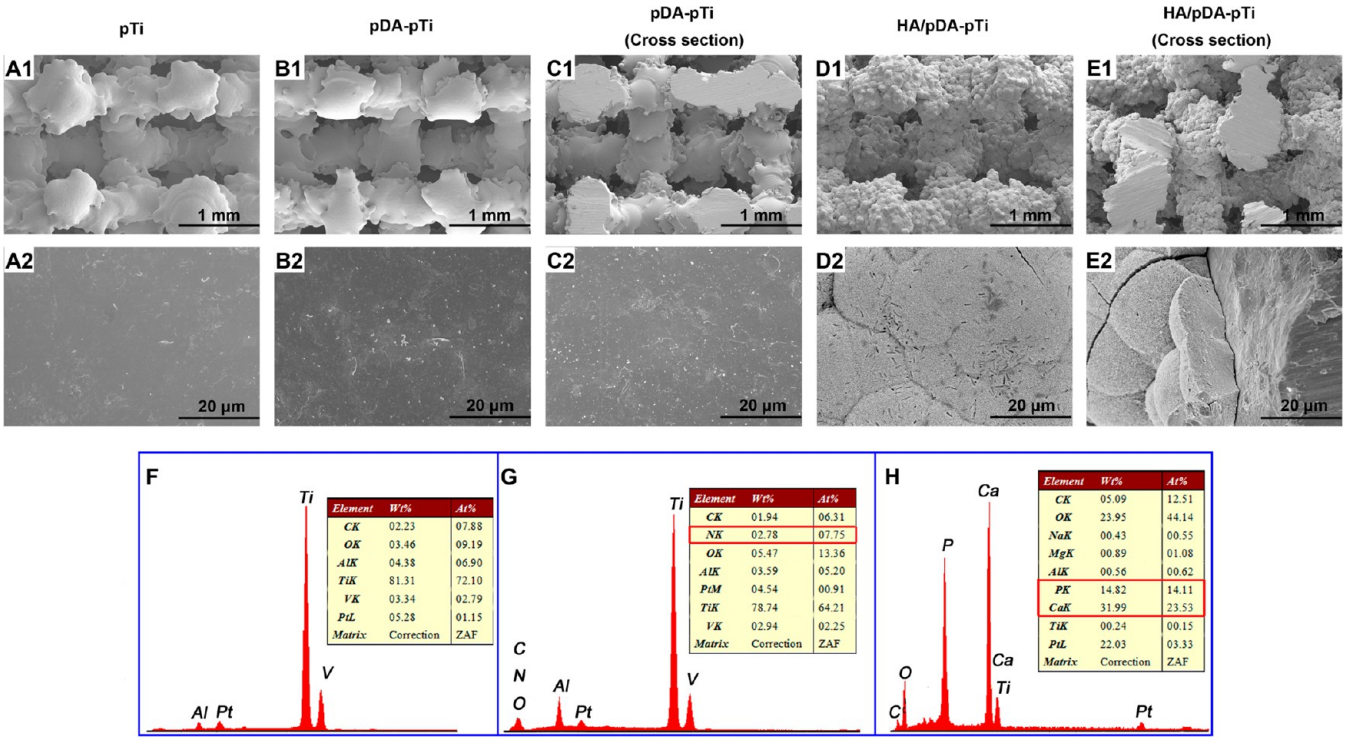

Figure 1. SEM images of (A1, A2) pTi, (B1, B2) pDA-pTi, (C1, C2) the cross section of pDA-pTi, (D1, D2) HA/pDA-pTi, and (E1, E2) the cross section of HA/pDA-pTi. EDS data for (F) pTi, (G) pDA-pTi, (H) HA/pDA-pTi. (G and H) The presence of nitrogen, calcium, and phosphorus elements in the EDS indicated that pDA and HA was successfully immobilized on the scaffolds. The resulting Ca/P ratio was 1.66, which is close to the theoretical ratio of HA (Ca/P = 1.67).

(OPN), and collagen type-1 (Col-1) were determined to evaluate the differentiation of the cultured cells. Total RNA was extracted from the cultured cells on the samples using the TRIzol reagent (Invitrogen Life Technologies) at each time point and subsequently converted into cDNA using PrimeScript RT Master Mix (Takara). The RT-PCR reactions were performed using SYBR Premix Ex Taq II (Takara) on the CFX96 PCR System (Bio-Rad). GAPDH was used as a housekeeping gene. The primers are shown in Table 1.

2.7. Animals and Surgical Procedures. For in vivo experiments, bare pTi, pDA-pTi, and HA/pDA-pTi samples were implanted into the lateral femoral epicondyle of male New Zealand white rabbits with an average weight of 2.5−3.5 kg (n = 6 in each group). Two different scaffolds were implanted into hind legs of each rabbit. The surgical procedures were performed as described previously.[44] The rabbits were anesthetized with phenobarbital sodium via intravenous injection. We shaved and sterilized the surgical areas and made an incision about 2 cm long to expose the lateral femoral epicondyle. A cylindrical defect (diameter, 5 mm; length, 10 mm) was then drilled on the lateral femoral epicondyle. Different scaffolds were inserted into the predrilled defects, then the incisions were closed with sutures and the surgical area was sterilized again. To prevent wound infection, each animal was given 40 000 U of penicillin per day via intramuscular injection for 3 days after surgery. All experimental procedures were approved by the ethics committee of the Fourth Military Medical University, according to the relevant guidelines and regulations.

2.8. Microcomputed Tomography (μCT) Analysis. After implantation for 4 and 12 weeks, the rabbits were sacrificed by intravenous injection of air under anesthesia. The femora condyles samples were harvested and fixed immediately by 4% paraformaldehyde in PBS for 7 days. The samples were scanned with Micron X-ray 3D Imaging System (Y.Cheetah, Germany) to determine the new bone formation. The X-ray source voltage was 90 kV, and the beam current was 50.0 μA. The scanning resolution is about 17 μm. The area of the implant was selected as the region of interest (ROI). The 450 projections were reconstructed using a modified parallel Feldkamp algorithm, and segmented into binary images (12-bit TIF images). The percentage of bone volume out of ROI (BV/TV) was calculated using the threshold of 200−1400 for bone and 1400−4095 for implant via VGStudio MAX software with beam hardening correction which can decrease metal artifacts in micro-CT results.

2.9. Histological Analysis. After the μCT analysis, the samples were dehydrated in graded ethanol solutions from 70 to 100% and finally embedded in methyl methacrylate (MMA). The embedded samples were sliced (about 50 μm in thickness) using a modified interlocked diamond saw (Leica Microtome, Wetzlar, Germany) and stained with 1.2% trinitrophenol and 1% acid fuchsin (Van-Gieson staining). The qualitative analysis of bone formation was performed with a standard light microscope (Leica LA Microsystems, Bensheim, Germany) and digital image analysis system (Image-Pro Plus software, Silver Spring, MD). Bone volume fraction (ratio of bone tissue area to the implant

DOI: 10.1021/acsami.5b00331
ACS Appl. Mater. Interfaces 2015, 7, 5715−5724

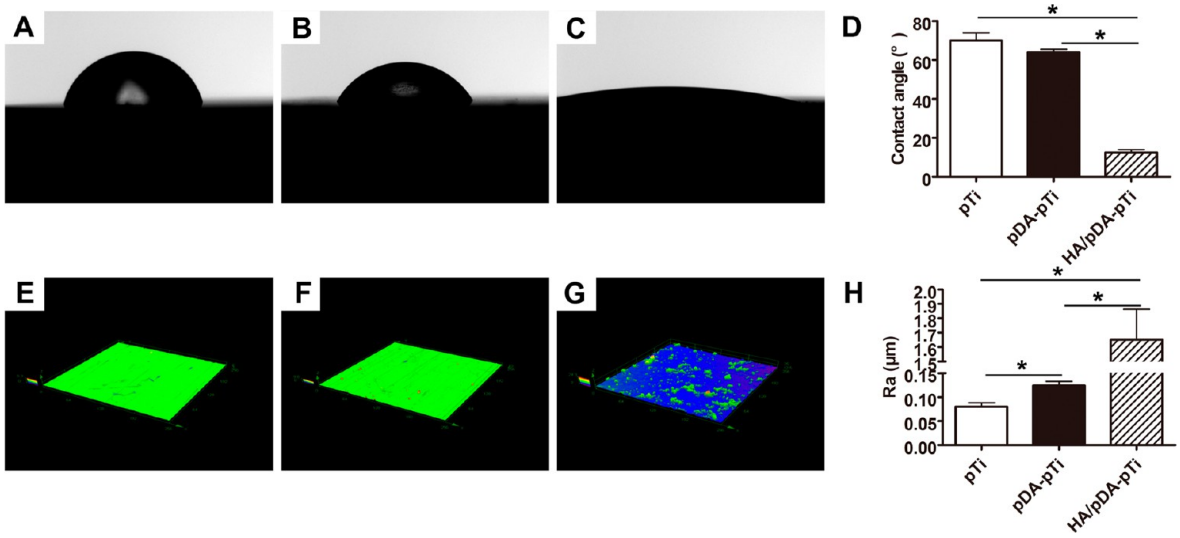

Figure 2. Water contact angle measurement for the (A) Ti6Al4V substrate, (B) Ti6Al4V substrate with pDA coating, and (C) Ti6Al4V substrate with HA/pDA coating. (D) Average water contact angle analysis. Surface CLSM images of the (E) Ti6Al4V substrate, (F) Ti6Al4V substrate with pDA coating, (G) Ti6Al4V substrate with HA/pDA coating. (H) Surface roughness analysis. For each group, $n = 3$; asterisks (*) indicate statistical significance, $p < 0.05$.

pore area within the implant) was calculated based on the Van-Gieson staining.

2.10. Statistical Analysis. The results were presented as the means ± SEM for each group. A one-way ANOVA followed by Bonferroni's multiple comparison tests were used to perform the statistical analysis among different groups. P value <0.05 was considered statistically significant.

3. RESULTS

3.1. Surface Characterization. The SEM images and EDS data showed that pDA (Figure 1B1,B2) and HA (Figure 1D1,D2) were successfully immobilized on the surfaces of pTi through a series of modifications. Especially, HA coating was clearly shown on the inner surfaces of the scaffold exposed by a horizontal dissection (Figure 1E1,E2). The change of surface morphology was not obvious under SEM after pDA immobilization (Figure 1A2,B2), while there is a significant change of surface morphology after HA coating (Figure 1A2,D1−E2). The presence of nitrogen element in the EDS (Figure 1G) indicated that pDA was successfully immobilized on the scaffolds. The presence of calcium and phosphorus elements (Figure 1H) indicated the successful coating of HA, and the resulting Ca/P ratio was 1.66, which is close to the theoretical ratio of HA (Ca/P = 1.67). HA was barely found on the scaffolds without pDA modification after soaking in SBF for 2 weeks (Supporting Information, Figure S1). Thus, pDA modification is critical to subsequent HA coating on the scaffolds.

After the pDA modification, water contact angles for the Ti6Al4V samples with pDA modification slightly decreased compared with the bare Ti6Al4V samples, but not statistically different (Figure 2A,B,D). However, the average water contact angle dramatically decreased from 70.13° (±3.83°) for the bare Ti6Al4V samples to 12.50° (±1.45°) for the Ti6Al4V samples with HA/pDA coating, indicating a significant increase of wettability by the HA coating on the scaffolds (Figure 2A,C,D). Moreover, it was found that the pDA coating first applied significantly increased the surface roughness of the scaffolds (Figure 2E,F,H), and the subsequent HA coating further substantially increased the surface roughness (Figure 2E,G,H).

Ti6Al4V samples with HA/pDA coating were treated with ultrasonication to evaluate the interfacial adhesion between the Ti6Al4V substrate and HA/pDA coating. About 85% of HA particles remained on the substrate surfaces after ultrasonication for an hour, and the pDA coating was confirmed to retain on the substrates (Supporting Information, Figure S2), which suggested that there was strong adhesion between the Ti6Al4V substrates and HA/pDA coating. The peeling test showed the similar result (about 83.5%), although there was disruption of the HA crystal (Supporting Information, Figure S2).

3.2. Cell Proliferation and Morphology. The cell proliferation was evaluated by the CCK-8 assay, which was found to increase with the increase of incubation time in both pTi and HA/pDA-pTi groups (Figure 3). Cell proliferation was

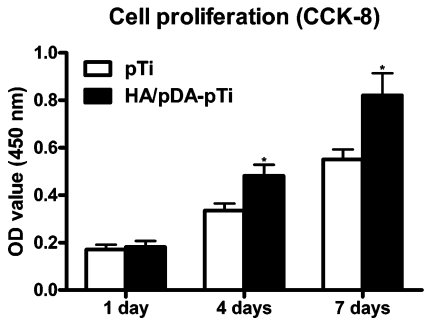

Figure 3. Measurement of MC3T3-E1 cells proliferation by CCK-8 assay after 1, 4, and 7 days incubation. For each group, $n = 3$; asterisks (*) indicate statistical significance compared to the pTi group, $p < 0.05$.

significantly greater in the HA/pDA-pTi group compared to pTi group at 4 and 7 days ($p < 0.05$, Figure 3). On the other hand, we found that there was no statistical difference in cell proliferation between the pTi and pDA-pTi groups (Supporting Information, Figure S3). Thus, these results indicated that HA coating fabricated by the biomimetic coating process promoted MC3T3-E1 cell proliferation on the porous Ti6Al4V scaffolds.

MC3T3-E1 cells were fluorescently stained for F-actin, vinculin and nuclei to investigate cell adhesion behavior. Cells

DOI: 10.1021/acsami.5b00331
ACS Appl. Mater. Interfaces 2015, 7, 5715−5724

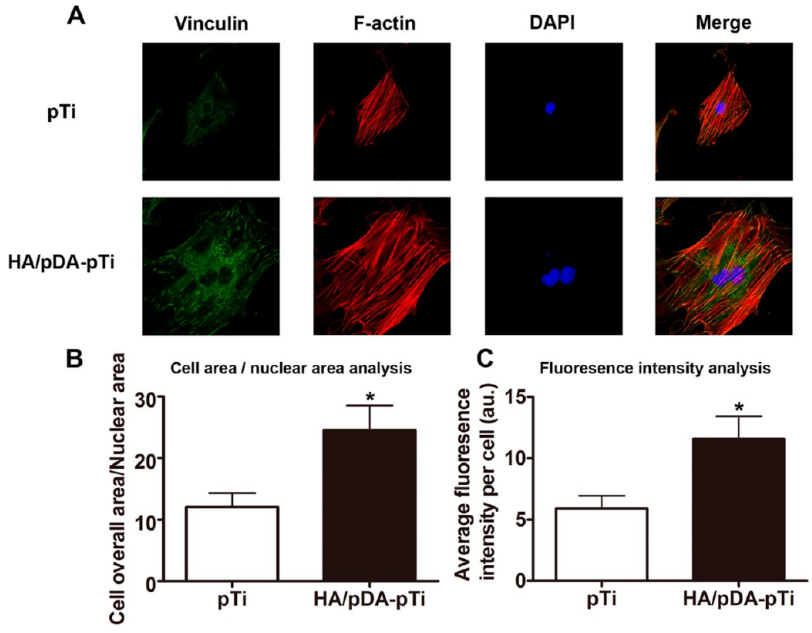

Figure 4. (A) Fluorescent staining of MC3T3-E1 cells adhered on pTi and HA/pDA-pTi scaffolds and (B) analysis of morphology and (C) fluorescence intensity of vinculin staining for cells on different scaffolds. (Three different fields were measured per sample, and three separate samples were measured for each group. Asterisks (*) indicate statistical significance compared to the pTi group, $p < 0.05$).

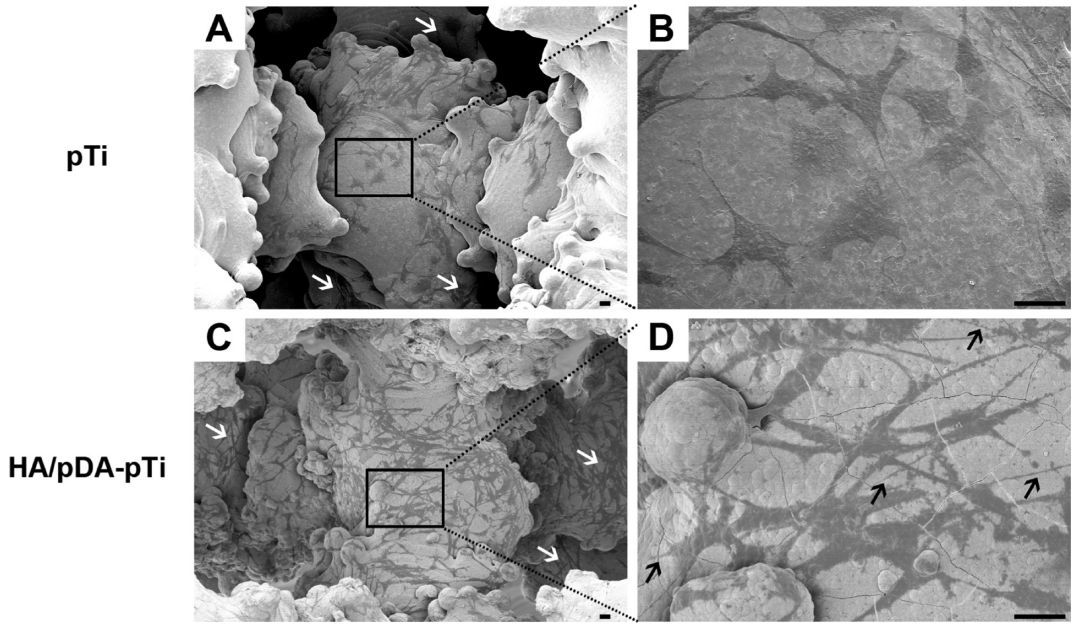

Figure 5. SEM images of MC3T3-E1 cells cultured on (A and B) pTi and (C and D) HA/pDA-pTi scaffolds for 4 days. White arrows indicate cells grown on the inner surfaces of the scaffolds, and black arrows indicate lamellipodia extensions. Scale bar = 100 μm.

on HA/pDA-pTi scaffolds spread better compared with those on bare pTi scaffolds (Figure 4A), and the cell overall area to the nucleus area (CN ratio) was higher in the HA/pDA-pTi group (Figure 4B). Additionally, cells from the HA/pDA-pTi group showed significantly higher fluorescence intensity of vinculin staining compared with those from the pTi group (Figure 4C). Both the cytoplasm and cell edges showed good distribution of vinculin in the HA/pDA-pTi group (Figure 4A), which likely contributed to the formation of focal adhesions.

SEM images showed that cells grew on the inner surfaces of both pTi and HA/pDA-pTi scaffolds (white arrows, Figure 5A,C), with a larger number of cells found in the latter group. Moreover, cells from the HA/pDA-pTi group displayed more lamellipodia extensions compared with the pTi group (black arrows, Figure 5B,D), suggesting that the HA/pDA coating promote cell migration.

3.3. Quantitative RT-PCR Tests. Cell differentiation was assessed at 7 and 14 days with osteogenic markers including Runx2, ALP, OCN, OPN, and Col-1 by quantitative RT-PCR tests. The levels of Runx2, ALP, and Col-1 gene expressions from the HA/pDA-pTi group were significantly higher compared with the pTi group at 7 and 14 days (Figure 6A,B,E). There was no significant difference for both OCN and OPN gene expressions at 7 days between the HA/pDA-pTi and pTi groups, while their

DOI: 10.1021/acsami.5b00331
ACS Appl. Mater. Interfaces 2015, 7, 5715−5724

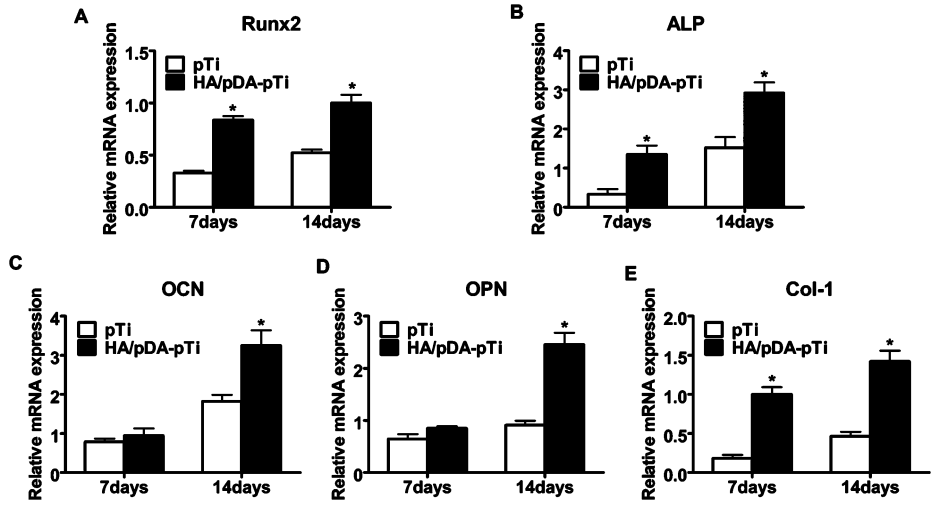

Figure 6. Relative mRNA expression of Runx2 (A), ALP (B), OCN (C), OPN (D) and Col-1 (E). (n = 3 for each group, asterisks (*) indicate statistical significance compared to the pTi group, $p < 0.05$).

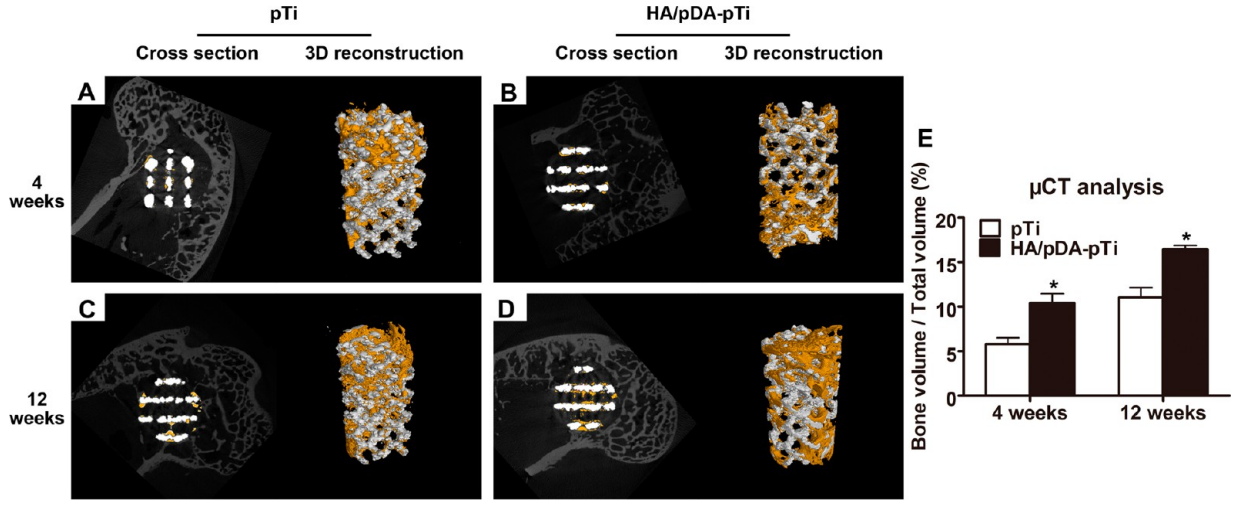

Figure 7. Micro-CT images of the pTi and HA/pDA-pTi implants at (A and B) 4 weeks and (C and D) 12 weeks, and the yellow color component was newly formed bone in these scaffolds. (E) Percentages of regenerated bone volume/total volume (BV/TV) in these implants. Asterisks (*) indicate statistical significance compared to the pTi group, $p < 0.05$.

gene expressions were significantly higher in the HA/pDA-pTi group at 14 days (Figure 6C,D). These results showed that the HA/pDA coating on the scaffolds promoted osteogenic differentiation of MC3T3-E1 cells.

3.4. Micro-CT and Histological Analysis. The growth of newly formed bone into scaffolds was characterized by μCT. The values of regenerated bone volume/total volume (BV/TV) increased with increase of implantation time in both HA/pDA-pTi and pTi groups (Figure 7A–E). Additionally, the BV/TV values were found to be significantly higher in the HA/pDA-pTi group compared with the pTi group at 4 weeks (Figure 7A,B,E) and 12 weeks (Figure 7C,D,E). However, there was no statistical difference for BV/TV values between pTi and pDA-pTi groups (Supporting Information, Figure S4). These results show that the biomimetic HA coating on the scaffolds was crucially important to bone regeneration.

The histological analysis based on the Van-Gieson staining was used to assess the osteogenesis and osteointegration of the pTi and HA/pDA-pTi implants. The results showed that trabeculae of the regenerated bone grown into the scaffolds were irregular at 4 weeks in both HA/pDA-pTi and pTi groups (Figure 8A1,A2,B1,B2), and thinner than the corresponding samples at 12 weeks (Figure 8C1,C2,D1,D2). Furthermore, the trabeculae of the newly formed bone were thicker in the HA/pDA-pTi group compared with those from the pTi group at 12 weeks (Figure 8C1,C2,D1,D2). In the pTi group, gaps were obviously found between the newly formed bone and scaffolds at 4 weeks (Figure 8A2,A3), and remained at 12 weeks (Figure 8C2,C3). On the other hand, excellent integration was found between the newly formed bone and scaffolds in the HA/pDA-pTi group (Figure 8D2,D3). Additionally, osteoblast seams with bone lining cells (marked by green arrows) were clearly shown at the interface between newly formed bone and the HA/pDA-pTi implant at 4 weeks (Figure 8B3), indicating active bone regeneration, and HA coating from the scaffold was also observed (marked by white arrows).

The volume of regenerated bone increased with increase of the implantation time (Figure 8E). Notably, the histomorphometric analysis revealed that the volumes of newly formed bone were significantly higher in the HA/pDA-pTi group compared with the pTi group at 4 weeks and 12 weeks (Figure 8E). In contrast, there was no statistical difference between pTi and pDA-pTi

DOI: 10.1021/acsami.5b00331
ACS Appl. Mater. Interfaces 2015, 7, 5715–5724

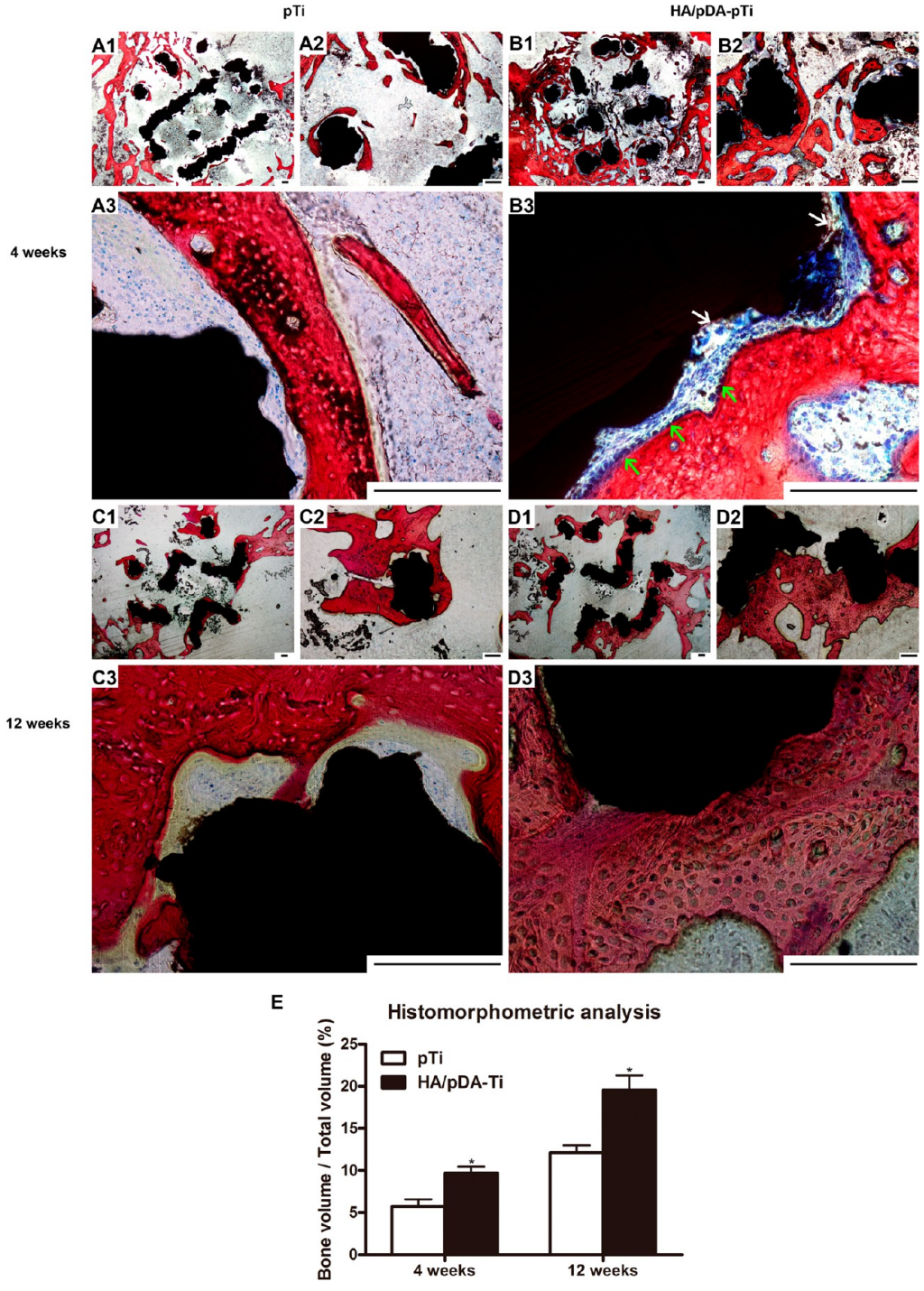

Figure 8. (A1−D3) Van-Gieson staining of histological sections and (E) histomorphometric analysis of the pTi and HA/pDA-pTi implants at 4 and 12 weeks postoperation. The tissue stained with red color was the newly formed bone. At 4 weeks, trabeculae of the new bone grown into scaffolds was irregular and thin (A1, A2, B1, and B2). Osteoblast seams with bone lining cells (marked by green arrows) as well as HA coating from the scaffold (marked by white arrows) can be seen at the interface between newly formed bone and the implant (B3), indicating active bone formation. Asterisks (*) indicate statistical significance compared to the pTi group, $p < 0.05$. Scale bar = 200 μm.

groups (Supporting Information, Figure S5). The above results revealed that the HA coating, not pDA coating substantially improved the osteogenesis and osteointegration property of porous Ti6Al4V scaffolds.

4. DISCUSSION

The porous titanium alloys with controllable pore size, geometry, and porosity can be fabricated by the advanced additive manufacturing techniques, which are attractive for use as substitutes for bone defect repair. However, how to improve the osteointegration and osteogenesis properties of these titanium scaffolds is a major concern for their clinical applications. HA coating is commonly employed to improve osteoconductivity and osteointegration of titanium scaffolds, which can mimic the nanoscale architecture and chemical composition of native bone mineral. However, it is still a

DOI: 10.1021/acsami.5b00331
ACS Appl. Mater. Interfaces 2015, 7, 5715−5724

challenge to obtain uniform HA coating onto the inner surfaces of porous Ti scaffolds. In this study, biomimetic coating of HA onto all surfaces of porous Ti6Al4V scaffolds was achieved following surface modification with pDA films formed by self-polymerization inspired by mussel-adhesion phenomena in nature. Our results showed that the resulting HA coating enhanced proliferation and osteogenic differentiation of MC3T3-E1 cells on the porous Ti6Al4V scaffolds in vitro and improved osteointegration and osteogenesis of the scaffolds in vivo.

A previous study revealed that pDA with structural mimic of the *Mytilus edulis* foot protein 5 (Mefp-5), a protein important for mussel attachment to wet surfaces, was able to form spontaneous deposition of thin films on various material surfaces.[20] This adhesive phenomenon was further found beneficial from the catecholamine moieties of pDA. Ryu et al. employed the pDA coating with abundant catecholamine moieties to assist HA formation on different scaffold materials.[42] Jo et al. showed that adhesion of MC3T3-E1 cells inside the 3D porous PCL scaffolds was enhanced by HA mineralization following pDA coating.[32] In this study, pDA-assisted HA coating was performed by a biomimetic coating process to improve osteointegration and osteogenesis of porous Ti6Al4V scaffolds fabricated by EBM. The pTi scaffolds were immersed into a dopamine solution and a 1.5× SBF solution in succession to modify all surfaces of the porous scaffolds. SEM and EDS results showed obvious changes of the surface morphology and element composition indicating the successful fabrication of HA/pDA-pTi scaffolds using the biomimetic coating method (Figure 1).

Previous studies showed that surface wettability and roughness were crucially important for cellular responses to the substrates.[19,45] We found that the water contact angle significantly decreased by HA coating on the Ti6Al4V scaffold (Figure 2), indicating that the surface wettability was substantially enhanced. Moreover, surface roughness increased after pDA immobilization and further significantly increased by the subsequent HA coating on the scaffolds (Figure 2). The ultrasonication test suggested that there was strong adhesion between the Ti6Al4V substrates and HA/pDA coating, which is important for implant. The CCK-8 assay showed that cell proliferation was promoted by the HA/pDA coating on the porous Ti6Al4V scaffolds (Figure 3). Moreover, cells grown on the HA/pDA-pTi scaffolds displayed greater intensity of vinculin staining (Figure 4) and more lamellipodia extensions (Figure 5) compared with those on the bare pTi scaffolds. Vinculin is a critical component for cell focal adhesions and plays an essential role in cell attachment, migration, and actin cytoskeleton formation.[45,46] Costa et al. demonstrated that surface morphology and roughness can influence vinculin expression in osteoblast cells.[45] Thus, the greater degree of vinculin staining and lamellipodia extension for cells on the HA/pDA-pTi scaffolds may be caused by change of surface morphology and roughness of the scaffold after the HA/pDA coating, which likely improves cell adhesion and migration.

Apart from cell adhesion and proliferation, cell differentiation is also critical for bone regeneration. The mRNA expressions of osteoblast-related genes (Runx2, ALP, OCN, OPN, and Col-1) were detected by quantitative RT-PCR to assess differentiation of MC3T3-E1 cells. It was found that the levels of Runx2, ALP, and Col-1 gene expressions were higher in the HA/pDA-pTi group compared with those from the pTi group at both 7 and 14 days, whereas the levels of OCN and OPN gene expressions were higher in the HA/pDA-pTi group only at 14 days, indicating HA/pDA coating promoted osteogenic differentiation of MC3T3-E1 cells. Thus, the in vitro study showed that the property of scaffold surfaces such as the chemical composition and surface wettability and roughness played an important role in cellular activities including adhesion, proliferation, and differentiation, which is consistent with previous studies.[45,47,48]

Furthermore, a rabbit femoral condylar defect model was developed to investigate osteointegration and osteogenesis property of these Ti6Al4V scaffolds in vivo. The HA/pDA-pTi group induced a larger volume of regenerated bone compared to the pTi group at 4 weeks and at 12 weeks, as shown by μCT results (Figure 7). Moreover, the Van-Gieson staining of histological sections showed that new bone actively formed around the HA/pDA-pTi scaffolds and demonstrated that the HA/pDA-pTi group had better osteointegration than the pTi group (Figure 8). These results indicated that HA/pDA coating improved the bioactivity of porous Ti6Al4V scaffolds, which is consistent with our in vitro findings and other studies.[49,50]

Thus, we herein demonstrate that pDA-assisted HA coating is a promising method to modify the surfaces of porous Ti6Al4V scaffolds for bone defect repair. The biomimetic coating process employed in this study is simple but time-consuming. In future work, this method should be improved to shorten the processing time, and the biological functions of the resulting HA/pDA coating need to be further investigated.

5. CONCLUSIONS

In this study, HA/pDA-pTi scaffolds were successfully fabricated through mussel-inspired pDA-assisted HA formation onto porous Ti6Al4V scaffolds using a biomimetic coating process, which showed uniform HA coating on the inner surfaces of the porous structures. In vitro studies including the CCK-8 assay, immunofluorescence staining and RT-PCR tests indicated that the HA/pDA coating on Ti6Al4V scaffolds promoted adhesion, proliferation, and differentiation of MC3T3-E1 cells compared with the bare pTi scaffolds. Moreover, μCT results of the implants and the Van-Gieson staining of histological sections revealed that HA/pDA-pTi scaffolds had greater osteointegration and osteogenesis property in vivo compared with the pTi scaffolds. Therefore, these biofunctionalized porous Ti6Al4V scaffolds are attractive for use as bone substitutes in orthopedic applications.

■ ASSOCIATED CONTENT

Supporting Information

SEM images of scaffolds after soaking in SBF for 2 weeks; ultrasonication test; cell proliferation of MC3T3-E1 cells on pTi and pDA-pTi scaffolds; micro-CT analysis of pTi and pDA-pTi scaffolds; and histomorphometric analysis of the pTi and pDA-pTi scaffolds. This material is available free of charge via the Internet at http://pubs.acs.org.

■ AUTHOR INFORMATION

Corresponding Author

*Phone: +86 29 84773411. Fax: +86 29 84773411. E-mail: guozheng@fmmu.edu.cn.

Author Contributions

[§]These authors contributed equally to this work.

Notes

The authors declare no competing financial interest.

DOI: 10.1021/acsami.5b00331
ACS Appl. Mater. Interfaces 2015, 7, 5715−5724

■ ACKNOWLEDGMENTS

This work was supported by the Research Fund for the National Natural Science Foundation of China (No. 51271199), the National Natural Science Foundation of China (No. 81171773), the National High-tech R&D Program (863 Program, No. 2015AA033702), and the Coordinative and Innovative Engineering Projects of Science and Technology of Shaanxi Province (No. 2012KTCG01-14).

■ REFERENCES

(1) Giannoudis, P. V.; Dinopoulos, H.; Tsiridis, E. Bone Substitutes: An Update. *Injury* **2005**, *36* (Suppl. 3), S20−27.

(2) Dimitriou, R.; Mataliotakis, G. I.; Angoules, A. G.; Kanakaris, N. K.; Giannoudis, P. V. Complications Following Autologous Bone Graft Harvesting from the Iliac Crest and Using the RIA: A Systematic Review. *Injury* **2011**, *42* (Suppl. 2), S3−15.

(3) Xue, W.; Krishna, B. V.; Bandyopadhyay, A.; Bose, S. Processing and Biocompatibility Evaluation of Laser Processed Porous Titanium. *Acta Biomater.* **2007**, *3*, 1007−1018.

(4) Murphy, C. M.; Haugh, M. G.; O'Brien, F. J. The Effect of Mean Pore Size on Cell Attachment, Proliferation and Migration in Collagen-glycosaminoglycan Scaffolds for Bone Tissue Engineering. *Biomaterials* **2010**, *31*, 461−466.

(5) Williams, J. M.; Adewunmi, A.; Schek, R. M.; Flanagan, C. L.; Krebsbach, P. H.; Feinberg, S. E.; Hollister, S. J.; Das, S. Bone Tissue Engineering Using Polycaprolactone Scaffolds Fabricated via Selective Laser Sintering. *Biomaterials* **2005**, *26*, 4817−4827.

(6) Simpson, R. L.; Wiria, F. E.; Amis, A. A.; Chua, C. K.; Leong, K. F.; Hansen, U. N.; Chandrasekaran, M.; Lee, M. W. Development of a 95/5 Poly(L-lactide-co-glycolide)/hydroxylapatite and Beta-Tricalcium Phosphate Scaffold as Bone Replacement Material via Selective Laser Sintering. *J. Biomed. Mater. Res., Part B* **2008**, *84*, 17−25.

(7) Duan, B.; Wang, M.; Zhou, W. Y.; Cheung, W. L.; Li, Z. Y.; Lu, W. W. Three-Dimensional Nanocomposite Scaffolds Fabricated via Selective Laser Sintering for Bone Tissue Engineering. *Acta Biomater.* **2010**, *6*, 4495−4505.

(8) Warnke, P. H.; Douglas, T.; Wollny, P.; Sherry, E.; Steiner, M.; Galonska, S.; Becker, S. T.; Springer, I. N.; Wiltfang, J.; Sivananthan, S. Rapid Prototyping: Porous Titanium Alloy Scaffolds Produced by Selective Laser Melting for Bone Tissue Engineering. *Tissue Eng., Part C* **2009**, *15*, 115−124.

(9) Pattanayak, D. K.; Fukuda, A.; Matsushita, T.; Takemoto, M.; Fujibayashi, S.; Sasaki, K.; Nishida, N.; Nakamura, T.; Kokubo, T. Bioactive Ti Metal Analogous to Human Cancellous Bone: Fabrication by Selective Laser Melting and Chemical Treatments. *Acta Biomater.* **2011**, *7*, 1398−1406.

(10) Amin Yavari, S.; van der Stok, J.; Chai, Y. C.; Wauthle, R.; Tahmasebi Birgani, Z.; Habibovic, P.; Mulier, M.; Schrooten, J.; Weinans, H.; Zadpoor, A. A. Bone Regeneration Performance of Surface-Treated Porous Titanium. *Biomaterials* **2014**, *35*, 6172−6181.

(11) Parthasarathy, J.; Starly, B.; Raman, S.; Christensen, A. Mechanical Evaluation of Porous Titanium (Ti6Al4V) Structures with Electron Beam Melting (EBM). *J. Mech. Behav. Biomed. Mater.* **2010**, *3*, 249−259.

(12) Wu, S. H.; Li, Y.; Zhang, Y. Q.; Li, X. K.; Yuan, C. F.; Hao, Y. L.; Zhang, Z. Y.; Guo, Z. Porous Titanium-6 Aluminum-4 Vanadium Cage Has Better Osseointegration and Less Micromotion than a Poly-ether-ether-ketone Cage in Sheep Vertebral Fusion. *Artif. Organs* **2013**, *37*, E191−201.

(13) Nguyen, H. The Effect of Sol−Gel-Formed Calcium Phosphate Coatings on Bone Ingrowth and Osteoconductivity of Porous-Surfaced Ti Alloy Implants. *Biomaterials* **2004**, *25*, 865−876.

(14) Lin, L.; Chow, K. L.; Leng, Y. Study of Hydroxyapatite Osteoinductivity with an Osteogenic Differentiation of Mesenchymal Stem Cells. *J. Biomed. Mater. Res., Part A* **2009**, *89*, 326−335.

(15) Choi, S. W.; Zhang, Y.; Thomopoulos, S.; Xia, Y. In Vitro Mineralization by Preosteoblasts in Poly(DL-lactide-co-glycolide) Inverse Opal Scaffolds Reinforced with Hydroxyapatite Nanoparticles. *Langmuir* **2010**, *26*, 12126−12131.

(16) Chai, Y. C.; Truscello, S.; Bael, S. V.; Luyten, F. P.; Vleugels, J.; Schrooten, J. Perfusion Electrodeposition of Calcium Phosphate on Additive Manufactured Titanium Scaffolds for Bone Engineering. *Acta Biomater.* **2011**, *7*, 2310−2319.

(17) Facca, S.; Lahiri, D.; Fioretti, F.; Messadeq, N.; Mainard, D.; Benkirane-Jessel, N.; Agarwal, A. In Vivo Osseointegration of Nano-designed Composite Coatings on Titanium Implants. *ACS Nano* **2011**, *5*, 4790−4799.

(18) Fu, Q.; Hong, Y.; Liu, X.; Fan, H.; Zhang, X. A Hierarchically Graded Bioactive Scaffold Bonded to Titanium Substrates for Attachment to Bone. *Biomaterials* **2011**, *32*, 7333−7346.

(19) Bayram, C.; Demirbilek, M.; Çalışkan, N.; Demirbilek, M. E.; Denkbcş, E. B. Osteoblast Activity on Anodized Titania Nanotubes: Effect of Simulated Body Fluid Soaking Time. *J. Biomed. Nanotechnol.* **2012**, *8*, 482−490.

(20) Lee, H.; Dellatore, S. M.; Miller, W. M.; Messersmith, P. B. Mussel-Inspired Surface Chemistry for Multifunctional Coatings. *Science* **2007**, *318*, 426−430.

(21) Sileika, T. S.; Kim, H. D.; Maniak, P.; Messersmith, P. B. Antibacterial Performance of Polydopamine-Modified Polymer Surfaces Containing Passive and Active Components. *ACS Appl. Mater. Interfaces* **2011**, *3*, 4602−4610.

(22) Fullenkamp, D. E.; Rivera, J. G.; Gong, Y. K.; Lau, K. H.; He, L.; Varshney, R.; Messersmith, P. B. Mussel-Inspired Silver-Releasing Antibacterial Hydrogels. *Biomaterials* **2012**, *33*, 3783−3791.

(23) Lee, H.; Rho, J.; Messersmith, P. B. Facile Conjugation of Biomolecules onto Surfaces via Mussel Adhesive Protein Inspired Coatings. *Adv. Mater.* **2009**, *21*, 431−434.

(24) Lai, M.; Cai, K.; Zhao, L.; Chen, X.; Hou, Y.; Yang, Z. Surface Functionalization of TiO_2 Nanotubes with Bone Morphogenetic Protein 2 and Its Synergistic Effect on the Differentiation of Mesenchymal Stem Cells. *Biomacromolecules* **2011**, *12*, 1097−1105.

(25) Lee, Y. B.; Shin, Y. M.; Lee, J. H.; Jun, I.; Kang, J. K.; Park, J. C.; Shin, H. Polydopamine-Mediated Immobilization of Multiple Bioactive Molecules for the Development of Functional Vascular Graft Materials. *Biomaterials* **2012**, *33*, 8343−8352.

(26) Chien, C. Y.; Tsai, W. B. Poly(dopamine)-Assisted Immobilization of Arg-Gly-Asp Peptides, Hydroxyapatite, and Bone Morphogenic Protein-2 on Titanium to Improve the Osteogenesis of Bone Marrow Stem Cells. *ACS Appl. Mater. Interfaces* **2013**, *5*, 6975−6983.

(27) Ko, E.; Yang, K.; Shin, J.; Cho, S. W. Polydopamine-Assisted Osteoinductive Peptide Immobilization of Polymer Scaffolds for Enhanced Bone Regeneration by Human Adipose-Derived Stem Cells. *Biomacromolecules* **2013**, *14*, 3202−3213.

(28) Nijhuis, A. W.; van den Beucken, J. J.; Boerman, O. C.; Jansen, J. A.; Leeuwenburgh, S. C. 1-Step versus 2-Step Immobilization of Alkaline Phosphatase and Bone Morphogenetic Protein-2 onto Implant Surfaces Using Polydopamine. *Tissue Eng., Part C* **2013**, *19*, 610−619.

(29) Ku, S. H.; Ryu, J.; Hong, S. K.; Lee, H.; Park, C. B. General Functionalization Route for Cell Adhesion on Non-wetting Surfaces. *Biomaterials* **2010**, *31*, 2535−2541.

(30) Hong, S.; Kim, K. Y.; Wook, H. J.; Park, S. Y.; Lee, K. D.; Lee, D. Y.; Lee, H. Attenuation of the in Vivo Toxicity of Biomaterials by Polydopamine Surface Modification. *Nanomedicine (Lond, U. K.)* **2011**, *6*, 793−801.

(31) Tsai, W. B.; Chien, C. Y.; Thissen, H.; Lai, J. Y. Dopamine-Assisted Immobilization of Poly(ethylene imine) Based Polymers for Control of Cell-Surface Interactions. *Acta Biomater.* **2011**, *7*, 2518−2525.

(32) Jo, S.; Kang, S. M.; Park, S. A.; Kim, W. D.; Kwak, J.; Lee, H. Enhanced Adhesion of Preosteoblasts inside 3D PCL Scaffolds by Polydopamine Coating and Mineralization. *Macromol. Biosci.* **2013**, *13*, 1389−1395.

(33) Luo, R.; Tang, L.; Zhong, S.; Yang, Z.; Wang, J.; Weng, Y.; Tu, Q.; Jiang, C.; Huang, N. In Vitro Investigation of Enhanced Hemocompatibility and Endothelial Cell Proliferation Associated with Quinone-Rich

DOI: 10.1021/acsami.5b00331
ACS Appl. Mater. Interfaces 2015, 7, 5715−5724

Polydopamine Coating. *ACS Appl. Mater. Interfaces* **2013**, *5*, 1704−1714.
(34) Cui, J.; Yan, Y.; Such, G. K.; Liang, K.; Ochs, C. J.; Postma, A.; Caruso, F. Immobilization and Intracellular Delivery of an Anticancer Drug Using Mussel-Inspired Polydopamine Capsules. *Biomacromolecules* **2012**, *13*, 2225−2228.
(35) Ou, J.; Wang, J.; Liu, S.; Zhou, J.; Ren, S.; Yang, S. Microtribological and Electrochemical Corrosion Behaviors of Polydopamine Coating on APTS-SAM Modified Si Substrate. *Appl. Surf. Sci.* **2009**, *256*, 894−899.
(36) Tsai, W. B.; Chen, W. T.; Chien, H. W.; Kuo, W. H.; Wang, M. J. Poly(dopamine) Coating of Scaffolds for Articular Cartilage Tissue Engineering. *Acta Biomater.* **2011**, *7*, 4187−4194.
(37) Chien, C. Y.; Liu, T. Y.; Kuo, W. H.; Wang, M. J.; Tsai, W. B. Dopamine-Assisted Immobilization of Hydroxyapatite Nanoparticles and RGD Peptides to Improve the Osteoconductivity of Titanium. *J. Biomed. Mater. Res., Part A* **2013**, *101*, 740−747.
(38) Liu, X.; Cao, J.; Li, H.; Li, J.; Jin, Q.; Ren, K.; Ji, J. Mussel-Inspired Polydopamine: a Biocompatible and Ultrastable Coating for Nanoparticles in Vivo. *ACS Nano* **2013**, *7*, 9384−9395.
(39) Liu, Y.; Chang, C. P.; Sun, T. Dopamine-Assisted Deposition of Dextran for Nonfouling Applications. *Langmuir* **2014**, *30*, 3118−3126.
(40) Sobocinski, J.; Laure, W.; Taha, M.; Courcot, E.; Chai, F.; Simon, N.; Addad, A.; Martel, B.; Haulon, S.; Woisel, P.; Blanchemain, N.; Lyskawa, J. Mussel Inspired Coating of a Biocompatible Cyclodextrin Based Polymer onto CoCr Vascular Stents. *ACS Appl. Mater. Interfaces* **2014**, *6*, 3575−3586.
(41) Lee, M.; Ku, S. H.; Ryu, J.; Park, C. B. Mussel-Inspired Functionalization of Carbon Nanotubes for Hydroxyapatite Mineralization. *J. Mater. Chem.* **2010**, *20*, 8848−8853.
(42) Ryu, J.; Ku, S. H.; Lee, H.; Park, C. B. Mussel-Inspired Polydopamine Coating as a Universal Route to Hydroxyapatite Crystallization. *Adv. Funct. Mater.* **2010**, *20*, 2132−2139.
(43) Kokubo, T.; Takadama, H. How Useful Is SBF in Predicting In Vivo Bone Bioactivity? *Biomaterials* **2006**, *27*, 2907−2915.
(44) Fukuda, A.; Takemoto, M.; Saito, T.; Fujibayashi, S.; Neo, M.; Yamaguchi, S.; Kizuki, T.; Matsushita, T.; Niinomi, M.; Kokubo, T.; Nakamura, T. In Vivo Performance of Novel Soybean/Gelatin-based Bioactive and Injectable Hydroxyapatite Foams. *Acta Biomater.* **2015**, *12*, 242−249.
(45) Costa, D. O.; Prowse, P. D.; Chrones, T.; Sims, S. M.; Hamilton, D. W.; Rizkalla, A. S.; Dixon, S. J. The Differential Regulation of Osteoblast and Osteoclast Activity by Surface Topography of Hydroxyapatite Coatings. *Biomaterials* **2013**, *34*, 7215−7226.
(46) Woodruff, M. A.; Jones, P.; Farrar, D.; Grant, D. M.; Scotchford, C. A. Human Osteoblast Cell Spreading and Vinculin Expression upon Biomaterial Surfaces. *J. Mol. Histol.* **2007**, *38*, 491−499.
(47) He, C.; Jin, X.; Ma, P. X. Calcium Phosphate Deposition Rate, Structure and Osteoconductivity on Electrospun Poly(L-lactic acid) Matrix Using Electrodeposition or Simulated Body Fluid Incubation. *Acta Biomater.* **2014**, *10*, 419−427.
(48) Hu, Y.; Cai, K.; Luo, Z.; Zhang, Y.; Li, L.; Lai, M.; Hou, Y.; Huang, Y.; Li, J.; Ding, X.; Zhang, B.; Sung, K. L. Regulation of the Differentiation of Mesenchymal Stem Cells in Vitro and Osteogenesis in Vivo by Microenvironmental Modification of Titanium Alloy Surfaces. *Biomaterials* **2012**, *33*, 3515−3528.
(49) Deplaine, H.; Lebourg, M.; Ripalda, P.; Vidaurre, A.; Sanz-Ramos, P.; Mora, G.; Prosper, F.; Ochoa, I.; Doblare, M.; Gomez Ribelles, J. L.; Izal-Azcarate, I.; Gallego Ferrer, G. Biomimetic Hydroxyapatite Coating on Pore Walls Improves Osteointegration of Poly(L-lactic acid) Scaffolds. *J. Biomed. Mater. Res., Part B* **2013**, *101*, 173−186.
(50) Thorfve, A.; Lindahl, C.; Xia, W.; Igawa, K.; Lindahl, A.; Thomsen, P.; Palmquist, A.; Tengvall, P. Hydroxyapatite Coating Affects the Wnt Signaling Pathway during Peri-implant Healing in Vivo. *Acta Biomater.* **2014**, *10*, 1451−1462.

DOI: 10.1021/acsami.5b00331
ACS Appl. Mater. Interfaces 2015, 7, 5715−5724